symmetry

MDPI

Communication

Deep Penetration of UV Radiation into PMMA and Electron Acceleration in Long Plasma Channels Produced by 100 ns KrF Laser Pulses

Vladimir D. Zvorykin *, Sergei V. Arlantsev, Alexey V. Shutov, Nikolay N. Ustinovskii and Polad V. Veliev

P. N. Lebedev Physical Institute, Leninskii Prospekt, 53, 119991 Moscow, Russia; arlantsev@mail.ru (S.V.A.); ash@lebedev.ru (A.V.S.); ustinovskiynn@lebedev.ru (N.N.U.); p.veliev@lebedev.ru (P.V.V.)
* Correspondence: zvorykin@sci.lebedev.ru

Abstract: Long (~1 mm), narrow (30−40 μm in diameter) corrugated capillary-like channels were produced in the axially symmetric 2D interaction regime of 100 ns KrF laser pulses with polymethylmethacrylate (PMMA) at intensities of up to 5×10^{12} W/cm^2. The channels extended from the top of a deep (~1 mm) conical ablative crater and terminated in a 0.5 mm size crown-like pattern. The modeling experiments with preliminary drilled capillaries in PMMA targets and Monte Carlo simulations evidenced that the crown origin might be caused by high-energy (0.1–0.25 MeV) electrons, which are much higher than the electron temperature of the plasma corona ~100 eV. This indicates the presence of an unusual direct electron acceleration regime. Firstly, fast electrons are generated due to laser plasma instabilities favored by a long-length interaction of a narrow-band radiation with plasma in the crater. Then, the electrons are accelerated by an axial component of the electrical field in a plasma-filled corrugated capillary waveguide enhanced by radiation self-focusing and specular reflection at the radial plasma gradient, while channel ripples serve the slowing down of the electromagnetic wave in the phase with electrons.

Keywords: 2D interaction of KrF laser radiation with PMMA; fast electron acceleration in laser-produced plasma-filled waveguide

Citation: Zvorykin, V.D.; Arlantsev, S.V.; Shutov, A.V.; Ustinovskii, N.N.; Veliev, P.V. Deep Penetration of UV Radiation into PMMA and Electron Acceleration in Long Plasma Channels Produced by 100 ns KrF Laser Pulses. *Symmetry* **2021**, *13*, 1883. https://doi.org/10.3390/sym13101883

Academic Editor: Fabio Sattin

Received: 10 September 2021
Accepted: 1 October 2021
Published: 6 October 2021

1. Introduction

Among the varieties of phenomena in the interaction between laser radiation and matter, the generation of high pressures and the acceleration of charged particles in laser plasma are of the greatest interest for a number of scientific and applied problems. These processes, which have different dependences on the intensity and wavelength of radiation, are directly related to the implementation of inertial confinement fusion (ICF) with laser heating, which was first suggested by N.G. Basov and O.N. Krokhin [1]. The ablation pressure increases with the intensity and decreases with the radiation wavelength as $p \propto I^{2/3}\lambda^{-2/3}$ in the assumption that the main part of the radiation energy is released near the critical plasma density and is transmitted to the ablation front due to electronic thermal conductivity, while Bremsstrahlung absorption in the plasma corona with subcritical density is small [2–5]. Other interaction models, where the main role, on the contrary, was assigned to reverse Bremsstrahlung absorption, give dependences of $p \propto I^{7/9}\lambda^{-2/9}$ [6] or $p \propto I^{7/9}\lambda^{-2/3}$ [7]. In the latter case, an increase in the absorption gradient for short-wavelength radiation is taken into account. Accounting for a radiative energy transfer in the theoretical model [8] does not change these scalings.

The efficiency of electron acceleration in a laser plasma, determined by the ponderomotive radiation pressure $p_r \propto I\lambda^2$, on the contrary, increases with the wavelength. This is why UV radiation is preferred in direct-drive ICF, based on the implosion of spherical shell capsules with deuterium-tritium (DT) fuel by the ablative pressure of plasma directly created by laser radiation [9]. Decreasing the wavelength reduces the risk of developing

plasma instabilities and the associated generation of fast ("superheated") electrons in a plasma corona at a typical radiation intensity of ~10^{14} W/cm^2 and pulse duration of ~20 ns [10]. Due to its large range, they warm up the fuel before the compressed stage, which prevents an achievement of the required highest density matter at the collapse of the capsule. On the contrary, in the ICF scheme with "fast ignition", electrons with an energy of ~1 MeV were generated by an additional high-intensity short laser pulse (~10^{19} W/cm^2, ~20 ps). They play a crucial role in heating the pre-compressed fuel to a required high temperature [11]. In another promising ICF scheme with "shock ignition", the additional heating of compressed DT fuel is provided by a strong shock wave (SW) converging to the center of the capsule, which is generated due to a sharp increase in radiation intensity up to ~10^{16} W/cm^2 in the rest 100–200 ps of the laser pulse [12]. High intensity at the final stage of the pulse significantly increases the generation of fast electrons with energies of ~100 keV in plasma, whose role is not yet completely clear at present. By warming up the fuel, they prevent compression: on the other hand, they transfer a part of energy to the SW and thereby provide higher pressure in the center of the capsule [13]. Note that very symmetrical laser irradiation is required to prevent the hydrodynamic instabilities development at the interfaces between an ablator, frozen and gaseous DT fuel and to avoid their mixing inside the spherical capsule [10].

The above considerations in favor of UV laser radiation for generating higher ablative pressure were confirmed in many experiments [7,14–19] with plane targets performed at various laser radiation wavelengths in the intensity range of $10^{11}-10^{14}$ W/cm^2. It should be noted that in these experiments, during an exposure to nanosecond laser pulses, the ablation front passed a distance in the condensed matter less than the size of the irradiated spot, i.e., the one-dimensional (1D) plane geometry of the ablation front propagation and the SW generated by it was realized. In our previous experiments with Al, Pb, graphite and polyethylene $(C_2H_4)_n$ targets at GARPUN KrF laser [20–22], pressures consistent with the above scaling were measured in the intensity range of 5×10^{11}–5×10^{12} W/cm^2 for 100 ns pulses and a focal spot of ~150 μm. The largest pressure value at an intensity of 5×10^{12} W/cm^2 reached 4 Mbar. For long pulse duration and axially symmetric two-dimensional (2D) interaction geometry, a new hydrodynamic regime with a 30-fold increase in the propagation velocity of the ablation front in targets was observed as caused by the radial squeezing out of the substance. As a result, a deep cone-shaped crater with a length of ~1 mm was formed in opaque graphite and aluminum targets which absorbed the UV light in a thin submicron layer.

In polymethylmethacrylate (PMMA), a range of KrF radiation is rather large, from tens to a hundred microns in dependence on manufacturing [23–26]. The ablation of PMMA proceeds via photochemical mechanisms with a low threshold for UV light; the lowest threshold of PMMA decomposition into a gaseous fraction is just 0.7 J/cm^2. Distinct features of the high-energy UV light interaction with PMMA observed in our experiments are: (i) a conical SW evidencing a 2D hydrodynamic regime; and (ii) a thin capillary-like channel with a diameter of 30-40 μm extending deep into the target up to ~1 mm from the top of the ablative crater (Figure 1). The microscope images were obtained with sample illumination by an unpolarized incoherent light source and in a projection scheme in the polarized light of copper vapor laser [20–22]. The formation of the capillary channel is explained by the pre-focusing of incident radiation nearby the crater top due to specular reflection by the plasma density gradient near the conical surface and the self-focusing of radiation transmitted through plasma in the PMMA [27].

In this paper, we focus on the effect which has not been discussed yet. In Figure 1a, one can see a "crown" at the end of the capillary channel. Numerical simulations and novel experiments with preliminary drilled capillaries in PMMA targets evidence that this crown-like pattern is presumably associated with a deceleration of fast electrons which are generated and accelerated in extended laser plasma, filling a conical crater and a long "post-crater" capillary channel.

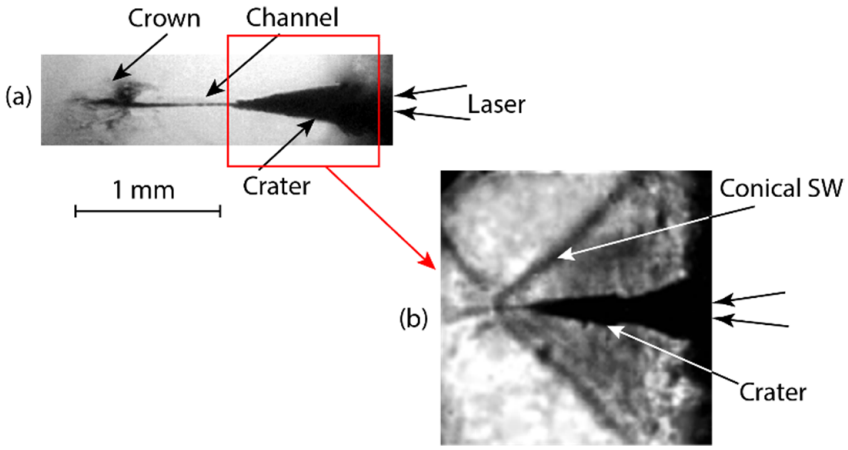

Figure 1. A side view of the crater produced in PMMA by 100 ns UV laser pulse with $I \approx 5 \times 10^{12}$ W/cm^2. The microscope images were obtained (**a**) with sample illumination by unpolarized incoherent light source; and (**b**) in the projection scheme in the polarized light of the copper vapor laser.

2. Performance of Experiments

The GARPUN KrF laser operated at a wavelength λ = 0.248 μm with an unstable telescopic resonator and a magnification parameter M = 6. A narrow-band ($\Delta\,\overline{v} \sim 0.1$ cm^{-1}) radiation of discharge pumped master oscillator Lambda Physik EMG 150 TMSC (200 mJ and 20 ns) was injected into the cavity and provided a narrow-band output of up to 100 J in 100 ns trapezoidal pulses with a rise front of 20 ns (for details see [27]). A slightly convergent output laser beam with an initial cross-section of 14 × 18 cm^2 was directed into the vacuum chamber and focused by a spherical mirror with F = 400 mm in a spot of a 150 μm diameter (at the 0.1 level of the maximum), which contained 75% of the whole energy.

The layout of the laser-target experiments is shown in Figure 2a. PMMA targets were parallelepipeds in form with a thickness (along a laser beam) of 3–5 mm and side surfaces with optical quality, through which the plasma glow inside the laser crater was recorded (Figure 2b). A plasma plume was imaged with a long focus length objective lens F = 210 mm in the intermediate plane, where an optical slit was placed. It cut out a narrow strip displayed by the second objective lens on the streak cameras "Agat" or PS-1/S1 (General Physics Institute of Russian Academy of Sciences—GPI RAS). They scanned in time the visible plasma glow in the direction perpendicular to the slit orientation. To adjust an actual horizontal plasma propagation along the laser beam in the case of the PS-1/S1 camera (where the scanning direction is horizontal), additional mirror optics rotated the image plane (it is not shown in Figure 2). A point light source was used to preliminarily align the optical scheme. Its radiation was collimated to probe the interaction region and to obtain target images at streak cameras in "idle mode", i.e., without scanning and in the absence of a laser shot. Precise target alignment was performed using a He–Ne laser, which illuminated the crater obtained in a previous laser shot. Images from an output screen of the Agat camera were registered with Spiricon SP620U profiler (Ophir Photonics). In the case of the PS-1/S1 camera, the images were registered with Anima-PX reader (Optronics Gmbh). Using the built-in software, the monochrome image on the screen was transformed into "pseudo-colors" corresponding to different intensity levels.

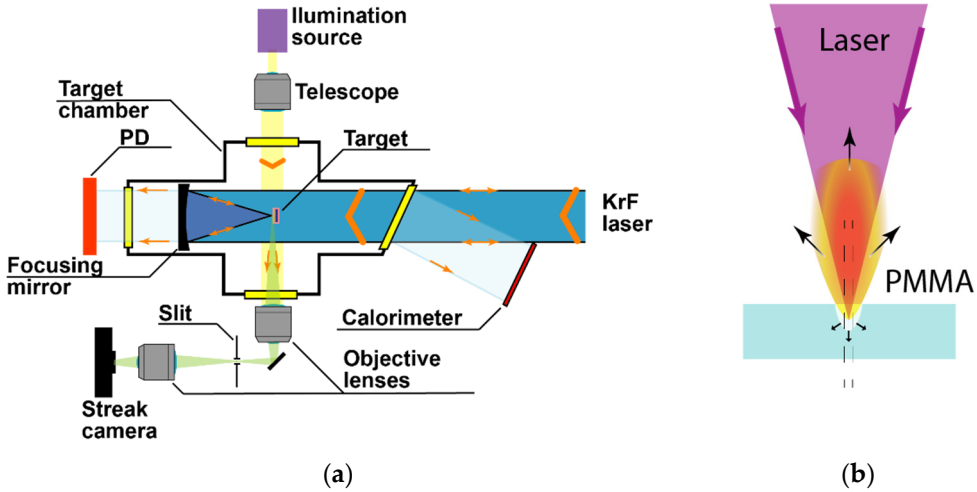

Figure 2. (**a**) Optical scheme for measuring the space–time dynamics of plasma glow and (**b**) a scheme for studying the interaction of laser pulses with PMMA targets.

3. Plasma Hydrodynamics for PMMA Targets

2D hydrodynamic interaction regime is clearly seen for the PMMA target irradiation image in Figure 3 obtained with a PS-1/S1 streak camera. When a 100 ns laser pulse with a peak intensity of 10^{12} W/cm^2 and a rise time of ~20 ns (see [27]) exposed a PMMA target, the maximum speed of plasma expansion into a residual gas of 100–150 km/s was achieved at the pulse plateau. By the end of the laser pulse, the propagation velocity of the plasma glow slowed down, which is obviously due to a rapid decrease in the density and temperature in the plasma corona as it expanded away from the target. An intense glow was also observed deep in the target propagating up to ~1 mm depth for 10–20 ns from the beginning of the laser pulse. It is much bigger than the focal spot diameter of 150 μm. This evidences a valumetric absorption of the UV laser light in a translucent PMMA material and very fast 2D ablation front propagation into the target. Over time, this inside glow gradually shifted to the target surface due to the increased absorption of the incident radiation in a plasma corona.

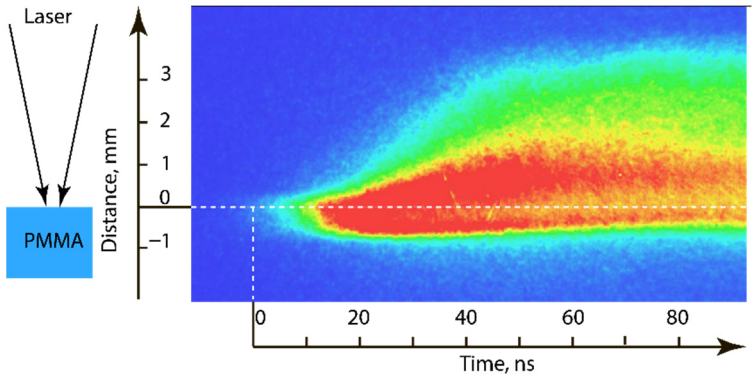

Figure 3. The spatio-temporal distribution of the plasma glow when the laser pulse with a peak radiation intensity $I \approx 10^{12}$ W/cm^2 exposed PMMA. The image was obtained with a PS-1/S1 streak camera.

A crater with a depth of up to 1 mm remained in the PMMA target after a laser pulse (Figure 1). When the next laser pulse struck the same crater produced by a previous pulse, radiation was absorbed in the target depth, and plasma glow moved deeper inside the target. This is clearly seen in the time-integrated (static) images of the PMMA glow obtained by displaying the target luminescence onto the profiler (Figure 4 on the left) and also on the space–time scans obtained with Agat streak camera (Figure 4 on the right).

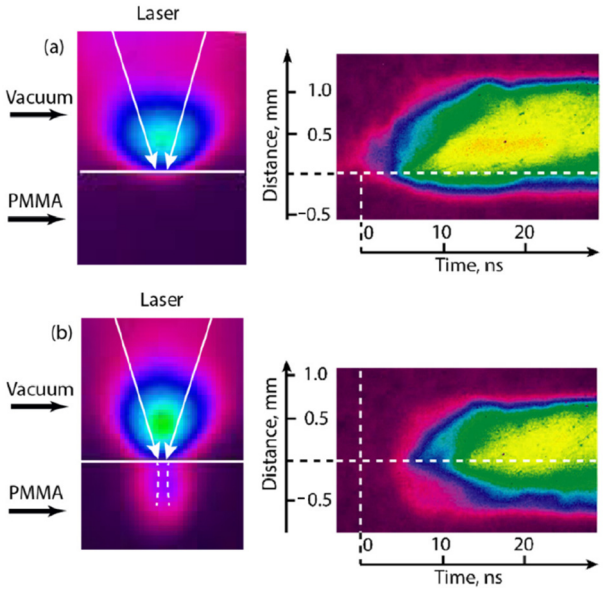

Figure 4. Plasma glow when (**a**) a laser pulse exposed the PMMA target and (**b**) the next laser pulse struck the same crater produced by the previous pulse. The peak radiation intensity was $I \approx 10^{12}$ W/cm^2. On the left are the time-integrated images; on the right are the space–time scanned images obtained with the Agat streak camera.

4. An Origin of the Crown Ending the Capillary Channel in PMMA

We believe that the crown-like pattern ending the 1 mm capillary channel in PMMA might be a multitude of deceleration tracks of an electron beam. Fast electrons could be generated as a result of a self-focusing of incident radiation in the deep ablative crater [27,28] and the development of laser plasma instabilities (LPI) favored by a long interaction length of a narrow-band laser radiation with underdense plasma [10,13]. Electrons could then be captured in the adjacent narrow capillary filled with plasma (Figure 5a). At an increased scale with an adjusted image intensity/contrast profile, the capillary in Figure 5b reveals a quasi-periodic structure with an axial period comparable with its diameter of 30–40 µm. The capillary channel resembles a corrugated plasma waveguide first considered by T. Tajima for a laser-driven plasma electron accelerator [29]. While hollow dielectric capillaries with a smooth wall or straight plasma-filled capillaries were shown to guide high-intensity laser radiation (see, e.g., [30,31]), the corrugated plasma capillary retarding the propagation of an electromagnetic laser field in phase with electrons effectively increases the acceleration length [32]. In our case, an interplay of laser radiation self-focusing in the plasma and specular reflection at a radial density gradient near the capillary wall creates a corrugated waveguide with an enhanced on-axis intensity profile and an electric field axial component which accelerates electrons along the capillary.

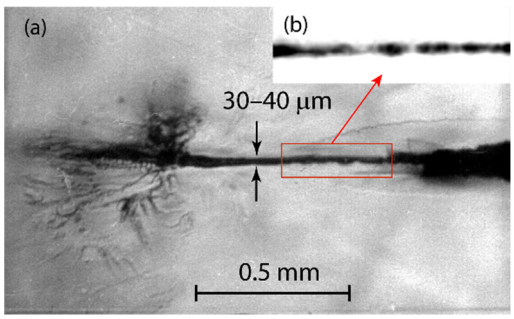

Figure 5. An image of (**a**) the capillary channel and crown produced in PMMA by UV laser pulse with $I \approx 5 \times 10^{12}$ W/cm^2; and (**b**) a fragment of the channel at an increased scale with an adjusted intensity/contrast profile.

Note that a quite different direct electron acceleration mechanism controls the acceleration process in a self-produced corrugated capillary channel at rather low laser intensity $I \leq 5 \times 10^{12}$ W/cm^2 in a long 100 ns UV laser pulse (λ = 0.248 μm) with a laser field parameter $a_0 = 8.5 \times 10^{-10}[I(\mathrm{W/cm^2})\lambda^2(\mu\mathrm{m}^2)]^{1/2} \ll 1$ compared with well-known laser-driven plasma-based acceleration regimes at relativistic intensities $I \geq 10^{18}$ W/cm^2 in femtosecond IR pulses ($\lambda \approx 1$ μm) with $a_0 \geq 1$ [33].

5. Monte Carlo Simulation of e-Beam Degradation in PMMA Targets

To validate the suggested model, numerical simulations were performed with the Monte Carlo code described elsewhere [34]. The code was further elaborated to simulate the coupled electron and bremsstrahlung X-ray transport through matter in the energy range from 0 to 1 MeV [35]. In this range, scattering cross-sections of the electrons and photons have a complex dependence on energy and cannot be described by analytical expressions. At the same time, for low-energy particles, the detailed structure of atomic shells becomes significant which requires the use of direct cross-section data. For this reason, the evaluated data library of Lawrence Livermore National Laboratory EPICS2014 distributed by the International Atomic Energy Agency (IAEA) [36] was chosen, which allowed better calculations of multiple electron trajectories and integrated energy deposition in PMMA samples. Approximately 50,000 histories were traced in simulations and the obtained trajectories of individual electrons are shown by various colors in Figure 6. The e-beam with an initial diameter of 30 μm was assumed, and began its interaction with PMMA at a 0.5 mm distance from the target front surface. Monoenergetic electron energy was varied in the range of 150–500 keV. Distributions of energy deposition in dependence of depth were obtained by integrating the energy losses of electrons over the radial coordinate and for the whole ensemble of particles (Figure 7).

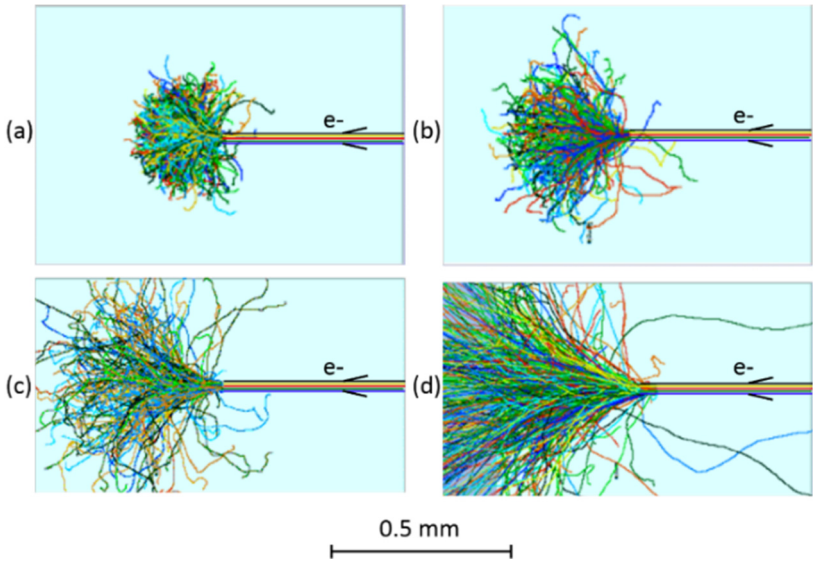

Figure 6. Monte Carlo simulations of individual electron trajectories in PMMA (approximately 50,000 histories are shown by various colors) for the initial e-beam diameter of 30 μm, with an electron energy of: (**a**) 150 keV; (**b**) 200 keV; (**c**) 250 keV; and (**d**) 500 keV. E-beam interaction with PMMA was assumed to begin at a 0.5 mm distance from the target front surface.

The comparison of the simulated results of e-beam scattering and absorption with the experimental pattern in Figure 5 shows that qualitative agreement with the crown form and size is achieved for the initial electron energy of approximately 200–250 keV.

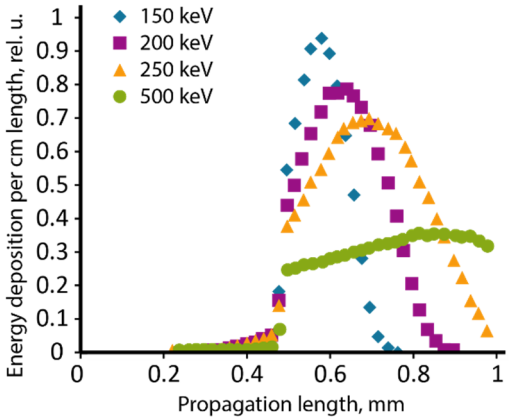

Figure 7. E-beam energy deposition per unit length depending on the depth of the PMMA integrated over a radial coordinate for 50,000 histories and different initial electron energy: 150, 200, 250 and 500 keV. It was assumed that the initial e-beam diameter of 30 μm and the interaction with PMMA began at a 0.5 mm distance from the target front surface.

6. The Modeling Experiments on Electron Acceleration in the PMMA Target with Preliminary Drilled Capillary

In this section, we describe the modeling experiments on electron acceleration in the PMMA target with a preliminary drilled capillary first reported at the LPpM3-2019 Conference [37]. The layout of these experiments is shown in Figure 8a. A high-aspect-ratio capillary was drilled in a PMMA sample by a discharge-pumped master oscillator EMG 150 TMSC operating with 1−2 mJ energy in 20 ns pulses at a 10 Hz repetition rate. Thus, PMMA targets with channels of 3 mm length and 30−40 μm diameter were produced (for details see [27]). Note an important distinction of these channels with a smooth wall from the above-discussed self-produced corrugated capillaries. A high-energy 100 ns UV pulse of GARPUN KrF laser was focused on the capillary inlet comparable in size with a spherical mirror focal spot and with an intensity of $I \approx 10^{12}$ W/cm^2. A stack of GAFCHROMIC radiochromic films set close to a capillary outlet served as an electron detector. To prevent film exposure by UV laser light, the stack was covered by 10 μm Al foil. The microscopic image of the PMMA sample after a laser shot (Figure 8b) shows a damaged area of approximately 2 mm in depth, formed by an SW energy load, and also the remainder of the capillary with a length of 1 mm.

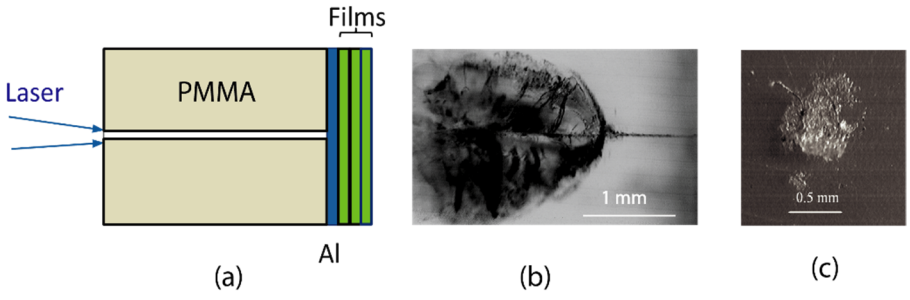

Figure 8. (**a**) A layout of experiments on electron acceleration in PMMA with a preliminary drilled channel; (**b**) a microscope image of the PMMA after irradiation by laser pulse with $I \approx 10^{12}$ W/cm^2; and (**c**) an imprint on the radiochromic film.

Although the protective Al foil survived after the laser shot, the emulsion layer was detached on the first and second films in the stack (Figure 8c). Assuming that the film destruction was caused exactly by electrons, their initial energy can be estimated from several tens to a hundred keV in a comparison of the tabulated data for the electron range [32] with the present attenuation in the combined thickness of the Al foil (10 μm)

and radiochromic films (~300 μm). These evidence a slightly lower accelerated electron energy than in the case of the self-produced corrugated capillaries. Although these are rather rough estimates, they nevertheless may confirm the importance of a corrugated capillary structure for more efficient electron accelerator.

7. Conclusions

The formation of a long (~1 mm) and a narrow (30−40 μm in diameter) capillary-like corrugated channel finished by a post-channel crown was observed in an axially symmetric 2D hydrodynamic regime, which is typical for the interaction of 100 ns UV laser pulses with a translucent PMMA targets at GARPUN KrF laser facility at intensities up to 5×10^{12} W/cm^2. A deep penetration of the UV radiation in PMMA and high ablation front velocities were confirmed by a spatial-temporal evolution of the visible plasma glow. The modeling experiments with a preliminary drilled capillary channel and Monte Carlo simulations evidence that the crown origin might be caused by an electron beam acceleration of up to a few hundred keV energies, which is much higher than the electron temperature of the plasma corona ~100 eV [21,22]. This indicates the presence of an unusual direct electron acceleration regime. It is supposed that electrons are firstly generated due to laser plasma instabilities favored by a long-length interaction of a narrow-band radiation with ablative plasma in a deep (~1 mm) crater. Electrons injected into a high-aspect-ratio self-produced corrugated plasma capillary are further accelerated by an axial component of the electrical field enhanced in a plasma-filled waveguide due to radiation self-focusing and specular reflection at radial density gradient, while channel ripples serve for slowing down the electromagnetic wave in phase with the electrons. Further experiments are underway to prove the alleged model.

Author Contributions: Conceptualization, V.D.Z.; methodology, V.D.Z.; software, S.V.A.; validation, V.D.Z. and S.V.A.; investigation, V.D.Z., A.V.S., P.V.V. and N.N.U.; writing—original draft preparation, V.D.Z.; writing—review and editing, S.V.A., A.V.S. and N.N.U. All authors have read and agreed to the published version of the manuscript.

Funding: This research was funded by the Russian Foundation for Basic Research (RFBR), grant number 19-02-00875.

Institutional Review Board Statement: Not applicable.

Informed Consent Statement: Not applicable.

Data Availability Statement: Not applicable.

Acknowledgments: We are grateful to Lebo I.G. from the Russian Technological University—MIREA—for the simulation of 2D laser plasma hydrodynamics and UV radiation self-focusing; and to Vorob'ev N.S. and Smirnov A.V. from GPI RAS for PS-1/S1 streak camera development and their assistance in measurements.

Conflicts of Interest: The authors declare no conflict of interest. The funders had no role in the design of the study; in the collection, analyses, or interpretation of data; in the writing of the manuscript, or in the decision to publish the results.

References

1. Basov, N.G.; Krokhin, O.N. Condition for heating up of a plasma by the radiation from an optical generator. *Sov. Phys. JETP* **1964**, *19*, 123–125.
2. Max, C.E.; McKee, C.F.; Mead, W.C. A model for laser driven ablative implosions. *Phys. Fluids* **1980**, *23*, 1620–1645. [CrossRef]
3. Mora, P. Theoretical model of absorption of laser light by a plasma. *Phys. Fluids* **1982**, *25*, 1051–1056. [CrossRef]
4. Manheimer, W.M.; Colombant, D.G.; Gardner, J.H. Steady-state planar ablative flow. *Phys. Fluids* **1982**, *25*, 1644–1652. [CrossRef]
5. Fabbro, R.; Max, C.; Fabre, E. Planar laser-driven ablation: Effect of inhibited electron thermal conduction. *Phys. Fluids* **1985**, *28*, 1463–1481. [CrossRef]
6. Dahmani, F.; Kerdja, T. Planar laser-driven ablation model for nonlocalized absorption. *Phys. Fluids B Plasma Phys.* **1991**, *3*, 1232–1240. [CrossRef]
7. Meyer, B.; Thiell, G. Experimental scaling laws for ablation parameters in plane target–laser interaction with 1.06 μm and 0.35 μm laser wavelengths. *Phys. Fluids* **1984**, *27*, 302–311. [CrossRef]

8. Basko, M.M.; Novikov, V.G.; Grushin, A.S. On the structure of quasi-stationary laser ablation fronts in strongly radiating plasmas. *Phys. Plasmas* **2015**, *22*, 053111. [CrossRef]
9. Nuckolls, J.; Wood, L.; Thiessen, A.; Zimmerman, G. Laser compression of matter to super-high densities: Thermonuclear (CTR) applications. *Nature* **1972**, *239*, 139–142. [CrossRef]
10. Craxton, R.S.; Anderson, K.S.; Boehly, T.R.; Goncharov, V.N.; Harding, D.R. Direct-drive inertial confinement fusion: A review. *Phys. Plasmas* **2015**, *22*, 110501. [CrossRef]
11. Tabak, M.; Hammer, J.; Glinsky, M.E.; Kruer, W.L.; Wilks, S.C. Ignition and high gain with ultrapowerful lasers. *Phys. Plasmas* **1994**, *1*, 1626–1634. [CrossRef]
12. Betti, R.; Zhou, C.D.; Anderson, K.S.; Perkins, L.J.; Theobald, W.; Solodov, A.A. Shock ignition of thermonuclear fuel with high areal density. *Phys. Rev. Lett.* **2007**, *98*, 155001. [CrossRef]
13. Tikhonchuk, V.T. Physics of laser plasma interaction and particle transport in the context of inertial confinement fusion. *Nucl. Fusion* **2019**, *59*, 032001. [CrossRef]
14. Grun, J.; Decoste, R.; Ripin, B.H.; Gardner, J. Characteristics of ablation plasma from planar, laser-driven targets. *Appl. Phys. Lett.* **1981**, *39*, 545–547. [CrossRef]
15. Key, M.H.; Toner, W.T.; Goldsack, T.J.; Kilkenny, J.D.; Veats, S.A. A study of ablation by laser irradiation of plane targets at wavelengths 1.05, 0.53, and 0.35 μm. *Phys. Fluids* **1983**, *26*, 2011–2026. [CrossRef]
16. Ng, A.; Pasini, D.; Celiiers, P.; Parfeniuk, L.; DaSilva, D.; Kwan, J. Ablation scaling in steady-state ablation dominated by inverse-bremsstrahlung absorption. *Appl. Phys. Lett.* **1984**, *45*, 1046–1048. [CrossRef]
17. Boehly, T.; Tanaka, K.A.; Mochizuki, T.; Yamanaka, C. Measurements of mass ablation rate and pressure in planar targets irradiated by 0.27-μm laser light. *J. Appl. Phys.* **1986**, *60*, 3840–3844. [CrossRef]
18. Dahmani, F. Ablation scaling in laser-produced plasmas with laser intensity, laser wavelength, and target atomic number. *Phys. Fluids B Plasma Phys.* **1992**, *4*, 1585–1588. [CrossRef]
19. Dahmani, F. Experimental scaling laws for mass-ablation rate, ablation pressure in planar laser-produced plasmas with laser intensity, laser wavelength, and target atomic number. *J. Appl. Phys.* **1993**, *74*, 622–634. [CrossRef]
20. Zvorykin, V.D.; Lebo, I.G. Laser and target experiments on KrF GARPUN laser installation at FIAN. *Laser Part Beams* **1999**, *17*, 69–88. [CrossRef]
21. Zvorykin, V.D.; Bakaev, V.G.; Korol, V.Y.; Lebo, I.G.; Rozanov, V.B.; Sychugov, G.V. Effects of anomalous high penetration rate of high-power KrF laser radiation throughout the solid matter and shock-induced graphite-diamond phase transformation. *Proc. SPIE* **2000**, *3885*, 212–222. [CrossRef]
22. Zvorykin, V.D.; Bakaev, V.G.; Lebo, I.G.; Sychugov, G.V. Hydrodynamics of plasma and shock waves generated by the high-power GARPUN KrF laser. *Laser Part. Beams* **2004**, *22*, 51–57. [CrossRef]
23. Srinivasan, R.; Braren, B.R.; Dreyfus, W.; Seeger, D.E. Mechanism of the ultraviolet laser ablation of polymethyl methacrylate at 193 and 248 nm: Laser-induced fluorescence analysis, chemical analysis, and doping studies. *J. Opt. Soc. Am. B* **1986**, *3*, 785–791. [CrossRef]
24. Philipp, H.R.; Cole, H.S.; Liu, Y.S.; Sitnik, T.A. Optical absorption of some polymers in the region 240–170 nm. *Appl. Phys. Lett.* **1986**, *48*, 192–194. [CrossRef]
25. Davis, G.M.; Gower, M.C. Time resolved transmission studies of poly(methyl methacrylate) films during ultraviolet laser ablative photodecomposition. *J. Appl. Phys.* **1987**, *61*, 2090–2092. [CrossRef]
26. Najeeb, H.N.; Balakit, A.A.; Wahab, G.A.; Kodeary, A.K. Study of the optical properties of poly (methyl methacrylate) (PMMA) doped with a new diarylethen compound. *Acad. Res. Int.* **2014**, *5*, 48–56.
27. Zvorykin, V.D.; Lebo, I.G.; Shutov, A.V.; Ustinovskii, N.N. Self-focusing of UV radiation in 1 mm scale plasma in a deep ablative crater produced by 100 ns, 1 GW KrF laser pulse in the context of ICF. *Matter Radiat. Extremes.* **2020**, *5*, 035401. [CrossRef]
28. Lebo, I.G. About the modeling of light beam self-focusing in plasma at the irradiation of the target by power UV laser. *Russ. Technol. J.* **2021**, *9*, 79–86. (In Russian) [CrossRef]
29. Tajima, T. High-energy laser plasma accelerators. *Laser Part. Beams* **1985**, *3*, 351–413. [CrossRef]
30. Cros, B.; Courtois, C.; Matthieussent, G.; Di Bernardo, A.; Batani, D. Eigenmodes for capillary tubes with dielectric walls and ultraintense laser pulse guiding. *Phys. Rev. E* **2002**, *65*, 026405. [CrossRef] [PubMed]
31. Spence, D.J.; Butler, A.; Hooker, S.M. First demonstration of guiding of high-intensity laser pulses in a hydrogen-filled capillary discharge waveguide. *J. Phys. B At. Mol. Opt. Phys.* **2001**, *34*, 4103–4112. [CrossRef]
32. Layer, B.D.; Palastro, J.P.; York, A.G.; Antonsen, T.M.; Milchberg, H.M. Slow wave plasma structures for direct electron acceleration. *New J. Phys.* **2010**, *12*, 095011. [CrossRef]
33. Esarey, E.; Schroeder, C.B.; Leemans, W.P. Physics of laser-driven plasma-based electron accelerators. *Rev. Mod. Phys.* **2009**, *81*, 1229–1285. [CrossRef]
34. Zvorykin, V.D.; Arlantsev, S.V.; Bakaev, V.G. Transport of electron beams and stability of optical windows in high-power e-beam-pumped krypton fluoride lasers. *Laser Part. Beams* **2001**, *19*, 609–622. [CrossRef]
35. Zvorykin, V.D.; Arlantsev, S.V.; Shutov, A.V.; Smetanin, I.V.; Ustinovskii, N.N. Delivery of the laser beam and transmissive optics degradation in KrF-based shock ignition inertial fusion energy approach. In *Pathways to Energy from Inertial Fusion: Structural Materials for Inertial Fusion Facilities, IAEA-TECDOC-1911*; International Atomic Energy Agency: Vienna, Austria, 2020; pp. 240–268.

36. EPICS2014 Electron and Photon Interaction Cross Sections. Available online: https://www-nds.iaea.org/epics2014/ (accessed on 1 September 2014).
37. Zvorykin, V.D.; Ustinovskii, N.N.; Shutov, A.V.; Lebo, I.G. Getting Long Ablation Channels in PMMA with Aspect Ratio ~1000 and Their Use in Experiments with Powerful KrF Laser Pulses. In Proceedings of the XVIII International Seminar "Mathematical Models & Modeling in Laser-Plasma Processes & Advanced Science Technologies"–LPpM3-2019, Petrovac, Montenegro, 29 September 2019; pp. 132–133. Available online: https://lppm3.ru/en/ (accessed on 1 September 2019).